Publ. Astron. Soc. Japan 2014 66 (4), 67 (1–22)
doi: 10.1093/pasj/psu038
Advance Access Publication Date: 2014 August 4

Study of negative and positive superhumps in ER Ursae Majoris

Tomohito Ohshima,[1,*] Taichi Kato,[1] Elena Pavlenko,[2] Hidehiko Akazawa,[3] Kazuyoshi Imamura,[3] Kenji Tanabe,[3] Enrique de Miguel,[4,5] William Stein,[6] Hiroshi Itoh,[7] Franz-Josef Hambsch,[6,8] Pavol A. Dubovsky,[9] Igor Kudzej,[9] Thomas Krajci,[10] Alex Baklanov,[2] Denis Samsonov,[2] Oksana I. Antonyuk,[2] Viktor Malanushenko,[2] Maksim V. Andreev,[11] Ryo Noguchi,[12] Kazuyuki Ogura,[12] Takashi Nomoto,[12] Rikako Ono,[12] Shin'ichi Nakagawa,[12] Keisuke Taniuchi,[12] Tomoya Aoki,[12] Miho Kawabata,[12] Hitoshi Kimura,[12] Kazunari Masumoto,[12] Hiroshi Kobayashi,[12] Katsura Matsumoto,[12] Kazuhiko Shiokawa,[13] Sergey Yu. Shugarov,[14,15] Natalia Katysheva,[14] Irina Voloshina,[14] Polina Zemko,[14] Kiyoshi Kasai,[13] Javier Ruiz,[16,17] Hiroyuki Maehara,[18] Natalia Virnina,[19] Jani Virtanen,[20] Ian Miller,[21] Boyd Boitnott,[6] Colin Littlefield,[22] Nick James,[23] Tamas Tordai,[24] Fidrich Robert,[24] Stefano Padovan,[25] and Atsushi Miyashita[26]

[1]Department of Astronomy, Kyoto University, Kitashirakawa-Oiwake-cho, Sakyo-ku, Kyoto 606-8502
[2]Crimean Astrophysical Observatory, 98409, Nauchny, Crimea, Ukraine
[3]Department of Biosphere-Geosphere System Science, Faculty of Informatics, Okayama University of Science, 1-1 Ridai-cho, Okayama, Okayama 700-0005
[4]Departamento de Física Aplicada, Facultad de Ciencias Experimentales, Universidad de Huelva, 21071 Huelva, Spain
[5]Center for Backyard Astrophysics, Observatorio del CIECEM, Parque Dunar, Matalascañas, 21760 Almonte, Huelva, Spain
[6]American Association of Variable Star Observers (AAVSO), C. E. Scovil Observatory, 2515 S. Summers Rd., Imlay City, MI 48444, USA
[7]Variable Star Observer's League in Japan (VSOLJ), 1001-105 Nishiterakata, Hachioji, Tokyo 192-0153
[8]Vereniging Voor Sterrnkunde (VVS), Oude Bleken 12, 2400 Mol, Belgium
[9]Vihorlat Observatory, Mierova 4, Humenne, Slovakia
[10]Astrokolkhoz Observatory, Center for Backyard Astrophysics (New Mexico), PO Box 1351, Cloudcroft, NM 83117, USA
[11]Institute of Astronomy, Russian Academy of Sciences, 361605 Peak Terskol, Kabardino-Balkaria, Russia
[12]Osaka Kyoiku University, 4-698-1 Asahigaoka, Kashiwara, Osaka 582-8582
[13]Variable Star Observer's League in Japan (VSOLJ), 405-1003 Matsushiro, Tsukuba, Ibaraki 305-0035
[14]Sternberg Astronomical Institute, Lomonosov Moscow University, Universitetskiy avenyu, 13, Moscow 119992, Russia
[15]Astronomical Institute of the Slovak Academy of Sciences, 05960, Tatranska Lomnica, The Slovak Republic
[16]Observatorio de Cantabria, Ctra. de Rocamundo s/n, Valderredible, Cantabria, Spain
[17]Agrupación Astronómica Cántabra (AAC), Apartado 573, 39080-Santander, Spain

[18]Kiso Observatory, Institute of Astronomy, School of Science, The University of Tokyo, 10762-30 Mitake, Kiso-machi, Kiso-gun, Nagano 397-0101
[19]Department of High and Applied Mathematics, Odessa National Maritime University, Ukraine
[20]Ollilantie 98, 84880 Ylivieska, Finland
[21]Furzehill House, Ilston, Swansea, SA2 7LE, UK
[22]Department of Physics, University of Notre Dame, Notre Dame, IN 46556, USA
[23]1 Tavistock Road, Chelmsford, Essex, CM1 6JL, UK
[24]Polaris Observatory, Hungarian Astronomical Association, Laborc utca 2/c, 1037 Budapest, Hungary
[25]American Association of Variable Star Observers (AAVSO), 49 Bay State Rd., Cambridge, MA 02138, USA
[26]Seikei Meteorological Observatory, Seikei High School, 3-3-1 Kichijoji-Kita-machi, Musashino, Tokyo 180-8633

*E-mail: ohshima@kusastro.kyoto-u.ac.jp

Received 2013 December 20; Accepted 2014 January 10

Abstract

We carried out photometric observations of the SU UMa-type dwarf nova ER UMa during 2011 and 2012, which showed the existence of persistent negative superhumps even during the superoutburst. We performed a two-dimensional period analysis of its light curves by using a method called "least absolute shrinkage and selection operator" (Lasso) and the "phase dispersion minimization" (PDM) analysis, and found that the period of negative superhumps systematically changed between a superoutburst and the next superoutburst. The trend of the period change can be interpreted as a reflection of the change of the disk radius. This change is in agreement with the one predicted by the thermal tidal instability model. The normal outburst during a supercycle showed a general trend that the rising rate to its maximum becomes slower as the next superoutburst is approaching. The change can be interpreted as the consequence of the increased gas-stream flow into the inner region of the disk as a result of the tilted disk. Some of superoutbursts were found to be triggered by a precursor normal outburst when the positive superhump appeared to develop. The positive and negative superhumps coexisted during the superoutburst. Positive superhumps were prominent only for four or five days after the supermaximum, while the signal of negative superhumps became stronger after the middle phase of the superoutburst plateau. A simple combination of the positive and negative superhumps was found to be insufficient for reproduction of the complex profile variation. We were able to detect the developing phase of positive superhumps (stage A superhumps) for the first time in ER UMa-type dwarf novae. Using the period of stage A superhumps, we obtained a mass ratio of 0.100(15), which indicates that ER UMa is on the ordinary evolutionary track of cataclysmic variable stars.

Key words: accretion, accretion disks — novae, cataclysmic variables — stars: dwarf novae — stars: individual (ER Ursae Majoris)

1 Introduction

Dwarf novae are a class of cataclysmic variables (CVs), which consist of a white dwarf primary and a late-type secondary which fills its Roche lobe. The material transferred toward the primary through the inner Lagrangian point (L1) forms an accretion disk around the white-dwarf. The accretion disk causes instabilities, which are observed as an outburst—for reviews, see Warner (1995), Osaki (1996), and Hellier (2001a). SU UMa-type stars are a subgroup of dwarf novae. They are characterized by the presence of two types of outbursts, normal outburst and superoutburst. Whereas a normal outburst lasts only a few days, a superoutburst lasts about two weeks and its maximum magnitude is brighter by 0.5–1 mag.

These objects also exhibit light variations called “(positive) superhumps” during their superoutburst. The observed period of such superhumps is a few percent longer than the orbital period of their system. The positive superhumps are thought to arise from periodic viscous dissipation of the tidally elongated disk (i.e., the eccentric disk) whose apsidal line slowly precesses in the prograde direction (see Whitehurst 1988; Hirose & Osaki 1990). On the other hand, some cataclysmic variables show variations, shorter than the orbital period, called “negative superhumps” (Udalski 1988; Harvey et al. 1995; Ringwald et al. 2012). The origin of negative superhumps is usually considered as a result of retrograde precession in a tilted accretion disk (Wood & Burke 2007). When the disk is tilted, the hot spot is formed at the inner part of the disk, not at the edge of the disk. Since the energy of the hot spot comes from the release of gravitational energy, such a change in the location of the hot spot causes a variation in the amount of released energy, namely, the luminosity of the hot spot. Combined with the retrograde precession, this effect can explain the negative superhump.

The interval of two successive superoutbursts is called a “supercycle.” Several normal outbursts are usually sandwiched between such superoutbursts. In order to explain such behavior of SU UMa-type dwarf novae, the thermal tidal instability (TTI) model was suggested (Osaki 1989). In this model, systems with a small mass ratio ($M_2/M_1 = q \leq 0.25$) enable the disk radius to reach the 3:1 resonance one of the orbital motion of the secondary. In normal outbursts, the material of the disk only partly accretes to the inner region. The radius of the disk becomes gradually larger after experiencing a normal outburst. When the disk radius reaches the 3:1 resonance one, the eccentric instability is excited. The increased turbulence in the disk increases the mass-transfer rate in the disk and a long, bright superoutburst is triggered (Osaki 1989). This prograde precession also causes the superhump (Whitehurst 1988; Hirose & Osaki 1990).

ER UMa is a member of the SU UMa-type dwarf nova and its superoutburst intervals (supercycles) are as short as 40–50 d (Kato & Kunjaya 1995). This object is known as the prototype of a subgroup, “ER UMa type,” which is characterized by having extremely short supercycles (<60 d) among SU UMa-type stars (e.g., Robertson et al. 1995; Nogami et al. 1995; for a review, see Kato et al. 1999). Although Gao et al. (1999) and Kjurkchieva and Marchev (2010) suggested the presence of negative superhumps during quiescence and a normal outburst, only positive superhumps were observed during the following superoutburst. However, Ohshima et al. (2012, hereafter Paper I) reported that negative superhumps were detected in ER UMa during the superoutburst in 2011 January. This is the first confident detection of negative superhumps during the superoutburst of an SU UMa-type dwarf nova. In Paper I, we reported on the detection of persistent negative superhumps in ER UMa and implied the possibility that the existence of negative superhumps suppresses the occurrence of normal outbursts.

The existence of negative superhumps during a superoutburst was also reported in other SU UMa-type dwarf novae, V1504 Cyg and V344 Lyr (Osaki & Kato 2013a; Still et al. 2010). Osaki and Kato (2013a) analyzed data of an SU UMa-type dwarf nova, V1504 Cyg, observed by Kepler, and showed that this object also shows negative superhumps during superoutbursts as well as during normal outbursts and its quiescence. Osaki and Kato (2013a) have demonstrated that in V1504 Cyg the frequency of occurrence of normal outbursts in a supercycle is related to the existence or nonexistence of negative superhumps in the sense that it is reduced when negative superhumps exist, confirming the suggestion made in Paper I. That is, the cycle length of normal outbursts in a supercycle with negative superhumps is longer than that without negative superhumps, and they called the former case a “type L supercycle” and the latter a “type S supercycle”—these types were first introduced by Smak (1985) for supercycles observed in VW Hyi and the symbols “L” and “S” come from “long” and “short” for normal outburst cycles.

In Paper I, we dealt with only one supercycle of ER UMa in 2011. We have made further comprehensive observations of ER UMa in 2011 and 2012, and our data covered three supercycles in 2011 and three in 2012. All of the supercycles observed have turned out to be accompanied with negative superhumps, and thus they provide an excellent opportunity to study the outburst behavior when negative and positive superhumps coexist. In this paper, we report on these new observations together with a more sophisticated analysis of the data reported in Paper I. We explain our observations in section 2, and present the result of their analysis in section 3. The conclusion is given in section 4.

2 Observations

We performed time-resolved photometric observations of ER UMa at 21 observatories scattered over the world from 2011 January to 2012 December with the VSNET Collaboration (Kato et al. 2004). We could obtain data on 146 nights in 2011, and 161 nights in 2012. The list of observatories is given in table 1, where the columns represent (1) the abbreviation of the observer, (2) the name of observer or

Table 1. List of observatories.

Key to observer	Observer or observatory name	Instruments*	Comparison star†
KU	Kyoto University	40 cmSCT+ST-9E	1
Aka	Akazawa Hidehiko	28 cmSC/35.5 cmSC + ST-7XE/ST-9XE	1,4,5
AKz	Astrokolkhoz team‡	30 cmSC+ST-9, 35 cmSC+ST-8	2
APO	Apache Point Observatory	50 cmC+SITe	6
BBo	Boyd Boitnott	28 cmSC+QSI-516wsg	6
CRI	Crimean Astrophy. Observatory	60 cm+Apogee Alta E47	6
deM	Enrique de Miguel	28 cmSC+QSI-516wsg, 25 cmL	2
DPV	Pavol A. Dubovsky	28 cmL+DSI ProII	6
Ham	Franz-Josef Hambsch	40 cm+STL11	2
Ioh	Itoh Hiroshi	30 cmSC+DSI-Pro-6	6
IMi	Ian Miller	35 cmSC+SXVR-H16	1,2,11
Kai	Kasai Kiyoshi	28 cmSC+ST-7XME	1,4
Kra	Tomas Krajci	28 cmSC+SBIG ST-8	6
LCO	Colin Littlefield	28 cmSC+ST-8XME	5,13,14
Mhh	Maehara Hiroyuki	25 cmL+ST-7XME	4
NDJ	Nick James	28 cmSC+SBIG ST-9XE	2
NKa	Natalia Katysheva	50 cmR/14 cmC+ST-10XME	1,2,4,6,8,9,10,12
OKU	Osaka Kyoiku Univ.	51 cm+ST-10	1
OUS	Okayama Univ. of Sci. team	23.5 cmSC+ST-8	6
PSD	Stefano Padovan	25 cm epsilon+ST-10XME	1,3,8,10,13,15
Pol	Polaris Observatory	ST-7E	4
Rui	Jevier Ruiz	0.4 mRC+ST-8XME	1
Sac	Seikei High School	15.2 cmR+ST-9E	5
Shu	Sergey Yu. Shugarov	50 cmR/14 cmC+ST-10XME	1,2,4,6,8,9,10,12
Siz	Siokawa Kazuhiko	35.5 cmSCT+ST-9E	4
SAO	Special Astrophys. Observatory§	1m+EEV CCD42-40’	1,2,4,6,8,9,10,12
SWI	William Stein	35 cmSCT+SBIG ST-10XME	2
Ter	Terskol Observatory	35 cmSCT+STL1001	6
Vir	Jani Virtanen	35 cmSCT+SBIG ST-10XME	6
VIR	Natalia Virnina	60 cm	6
Vol	Irina Voloshina	60 cmL+Apogee 47	11

*SCT: Schmidt-Cassegrain, R: Refractor, L: Reflector, C: Cassegrain, epsilon: Epsilon type astrograph.
†1: GSC 3439.629, 2: GSC 3439.920, 3: GSC 3439.1287, 4: TYC2-3439.1099.1, 5: TYC3439.1253.1, 6: GSC 3439.669, 7: GSC 3439.816, 8: GSC 3439.957, 9: GSC 3439.1211, 10: GSC 3439.745, 11: USNO1350.07816004, 12: GSC 3439.1105, 13: GSC 3439.911, 14: TYC2-3439.916.1, 15: GSC 3439.1091, 16: GSC 3439.885.
‡By F.-J. Hambsch and T. Krajci.
§By Natalia Katysheva.

observatory, (3) instruments used, and (4) comparison stars used. The list of all observations (table 4) and the maximum timings of negative superhumps (tables 5–10) are given only on the electronic version.[1] The chart of ER UMa and its comparison stars is presented in figure 1.[2]

After dark-subtracting and flat-fielding in CCD observations, we performed aperture photometry of the variable and its comparison stars, and obtained their differential magnitudes. The observed time was transformed to barycentric Julian Date (BJD). We made corrections for systematic differences among observers after that.

[1] ⟨http://dx.doi.org/10.1093/pasj/psu038⟩.

[2] Derived from ⟨http://cas.sdss.org/dr7/en/tools/chart/chart.asp⟩.

3 Result

In this section, we first present the results of our observations and their analysis, and then discuss their implications. We first describe the outburst behaviors of ER UMa in subsection 3.1, and then discuss its negative superhumps and positive superhumps in subsections 3.2 and 3.3, respectively. Finally we deal with the transition from negative superhump to positive superhump in subsection 3.4.

3.1 Outburst light curves

3.1.1 Overall light curves of ER UMa in 2011 and 2012

The overall light curve of ER UMa is presented in figure 2, for 2011, and figure 3, for 2012. The list of observed

Table 2. List of superoutbursts.

ID	Superoutburst start date (BJD−2400000.0)	Superoutburst maximum date (BJD−2400000.0)	Maximum magnitude	Supercycle length (d)
2011 S1	55578*	—	12.6*	—
2011 S2	55622.0	55625.1	12.7	44
2011 S3	55671.9	55674.4	12.7	50
2012 S1	55927†	55929†	12.9	58‡
2012 S2	55981.3	55982.6	13.0	54
2012 S3	56033.8	56034.4	12.9	53
2012 S4	—	56088.9§	—	55

*Based on VSNET data.
†The precise timing is unclear because of a scarcity of observations.
‡The date of the previous superoutburst is based on VSNET data.
§Estimated time of maximum, not the start of a outburst (due to a scarcity of observations).

Table 3. List of normal outbursts.

ID	Cycle length* (d)	Outburst start date (BJD−2400000.0)	Maximum magnitude
2011 N1-1	—	55592.2	13.6
2011 N1-2	5.7	55597.9	13.5
2011 N1-3	6.6	55604.5	13.4
2011 N1-4	6.6	55611.1	14.3
2011 N1-5	4.0	55615.1	13.3
2011 N2-1	—	55644.7	13.6
2011 N2-2	5.5	55650.2	13.4
2011 N2-3	6.7	55656.9	13.5
2011 N2-4	7.2	55664.1	13.2
2011 N3-1	—	55693.3	13.7
2011 N3-2	4.8	55698.1	13.6
2011 N3-3	7.4	55705.5	13.6‡
2011 N3-4	6.8	55712.3	13.4
2011 N3-5†	9.0‡	55721.3	13.2‡
2012 N0-1	—	55900.5	13.6
2012 N0-2	9.0	55909.5	13.5
2012 N0-3	9.5	55919.0	13.4
2012 N1-1	—	55946.3	13.9
2012 N1-2	5.9	55952.2	13.7
2012 N1-3	8.9	55961.1	13.8
2012 N1-4	8.0	55969.1	13.5
2012 N2-1	—	55998.8	13.5
2012 N2-2	5.9	56004.7	13.9
2012 N2-3	8.2	56012.9	13.9
2012 N2-4	9.3	56022.2	13.5
2012 N2-5	9.4	56031.6§	13.5
2012 N3-1	—	56051.0‖	13.7
2012 N3-2	6.4	56057.4‖	13.8
2012 N3-3	6.5	56063.9‖	13.7
2012 N3-4	6.7	56070.6‖	13.7
2012 N3-5	11.3	56081.9‖	14.2

*The cycle length ranging from the previous outburst to the current one.
†Suspected superoutburst.
‡Not confirmed.
§Precursor outburst of the next superoutburst.
‖Estimated time of maximum, not the start of the outburst (due to a scarcity of observations).

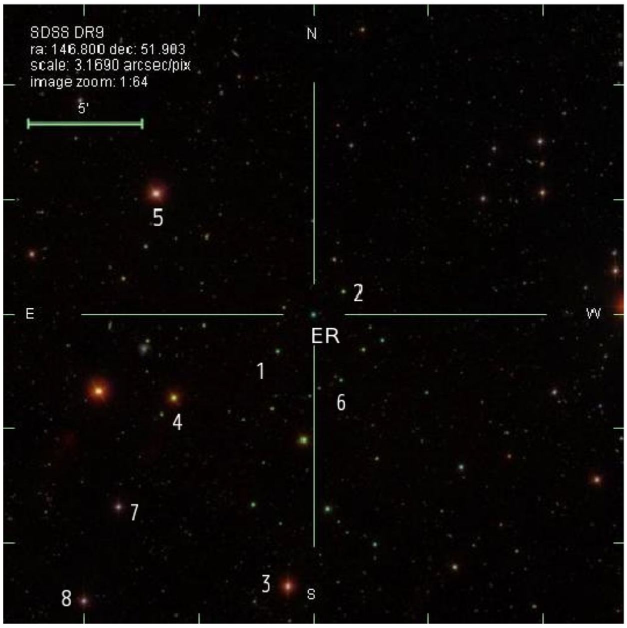

Fig. 1. Finding chart of ER UMa and its comparison stars. (Color online)

superoutbursts is shown in table 2, where the columns represent (1) the identification of superoutburst, (2) its starting date in BJD, (3) the BJD of the supermaximum, (4) the magnitude at its maximum, and (5) the length of supercycle, where the supercycle is defined as the period from the starting date of the previous superoutburst to that of the current one. As can be seen in figures 2 and 3, three superoutbursts in 2011 (2011 S1–S3) and three superoutbursts in 2012 (2012 S1–S3) were clearly observed during this observational campaign. Although a candidate for superoutburst was also observed in 2012 (2012 S4), it was unclear because of sparse data points. The lengths of observed supercycles were within the range of 44–58 d. These values are in agreement with those in the previous report (Zemko et al. 2013). Table 3 shows the list of normal outbursts. The first

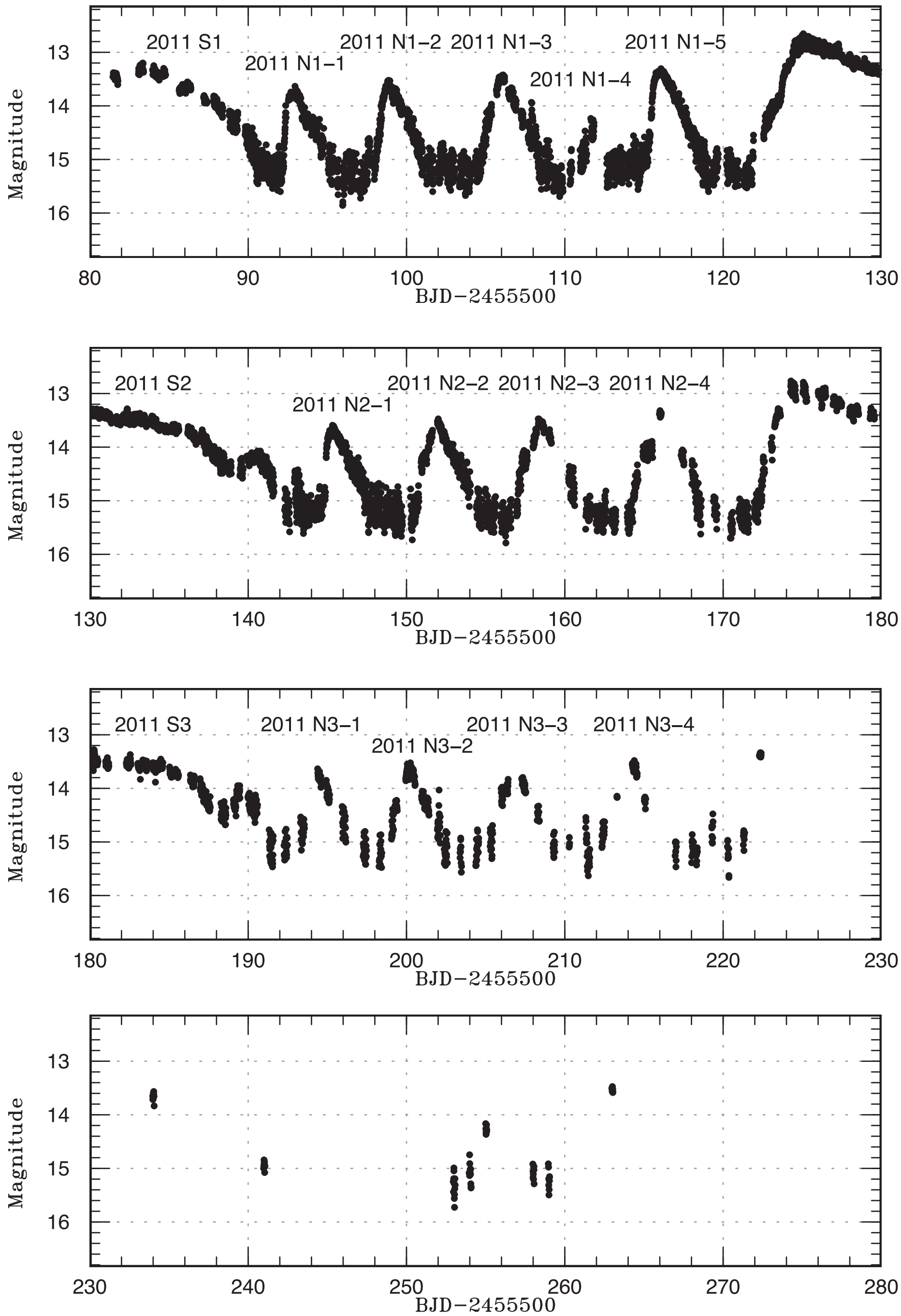

Fig. 2. All light curves of ER UMa observed in the 2011 season. The data are binned to 0.01 d.

column is the identification of normal outburst. Here, 2012 N2-3, for instance, indicates the third normal outburst in supercycle No. 2 in 2012. We see from table 3 that the maximum magnitude of normal outbursts becomes brighter and the cycle length of normal outburst becomes longer as the outburst behavior approaches the next superoutburst (i.e., with the development of supercycle phase), although some exceptions do exist (e.g., the interval between 2012 N1-2 and N1-3 is longer than that between 2012 N1-3 and N1-4).

3.1.2 Description of individual supercycles

Let us now examine the outburst behavior of individual supercycles. Here we define a supercycle by the identification of the starting superoutburst in a supercycle; that is, "supercycle 2011 S1", for instance, is a supercycle which begins with the superoutburst 2011 S1 and ends with 2011 S2. The duration of a superoutburst is defined as the period from its maximum time to its end time, because observations in the rising stage were lacking in some cases.

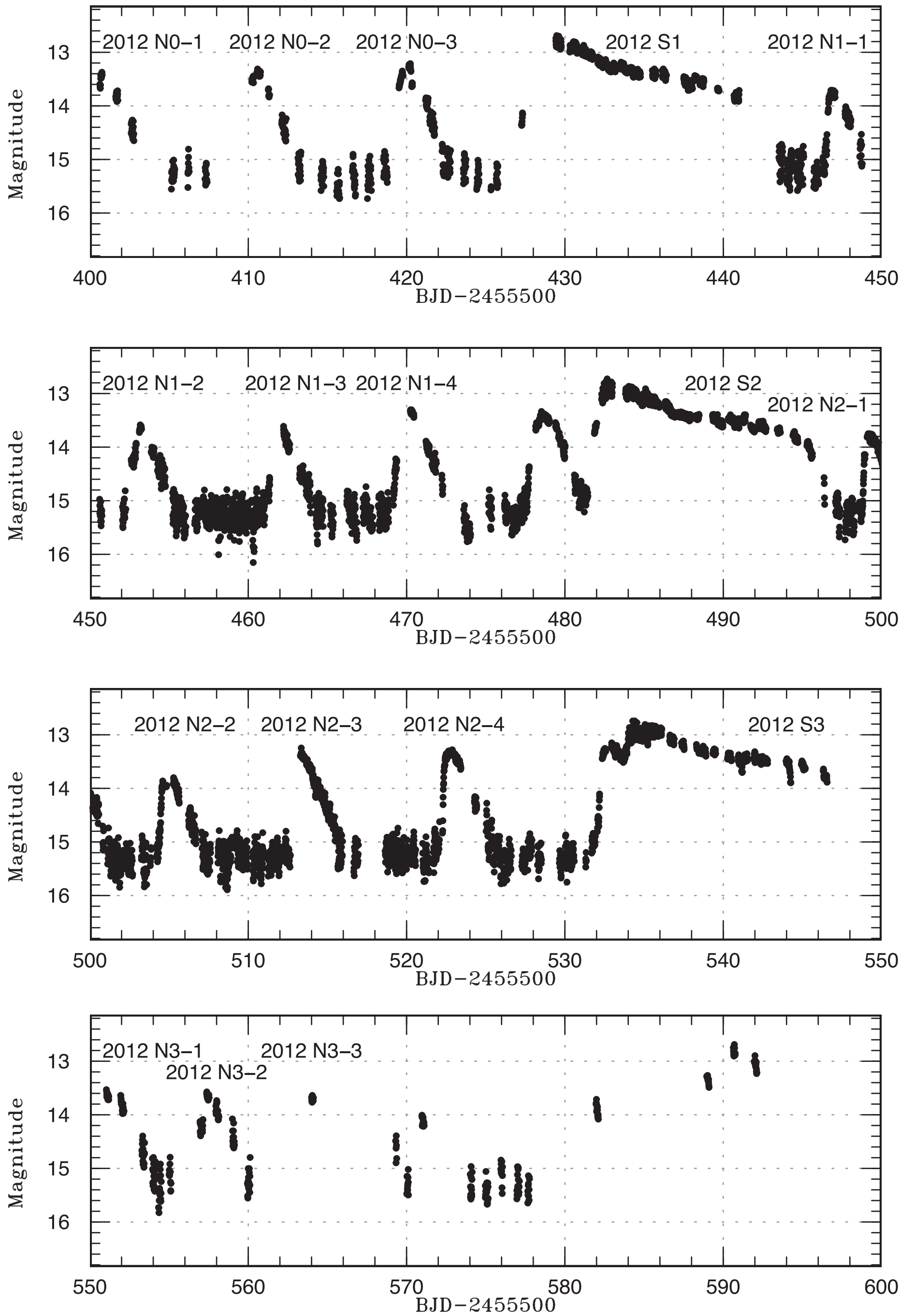

Fig. 3. All light curves of ER UMa observed in the 2012 season. The data are binned to 0.01 d.

Supercycle 2011 S1: This was the first superoutburst during which negative superhumps were detected for the first time (Paper I). Time-resolved observations started three days after the detection of the superoutburst. Unfortunately, its rising part was not observed and the existence of positive superhumps in this superoutburst was not confirmed. However, we suspect that the positive superhumps must have appeared, most likely in its earliest phase.

The superoutburst lasted probably 13–15 d. Two days after its end, the next normal outburst (2011 N1-1) started. In this supercycle, this object had four normal outbursts (start dates: BJD 2455592.2, 2455597.9, 2455604.5, and 2455615.1). Besides these, a minioutburst with an amplitude of only 1 mag occurred (BJD 2455611.1). The length of the supercycle was 44 d.

Supercycles 2011 S2 and 2011 S3: Superoutburst 2011 S2 started as a form of normal outburst; the start of the

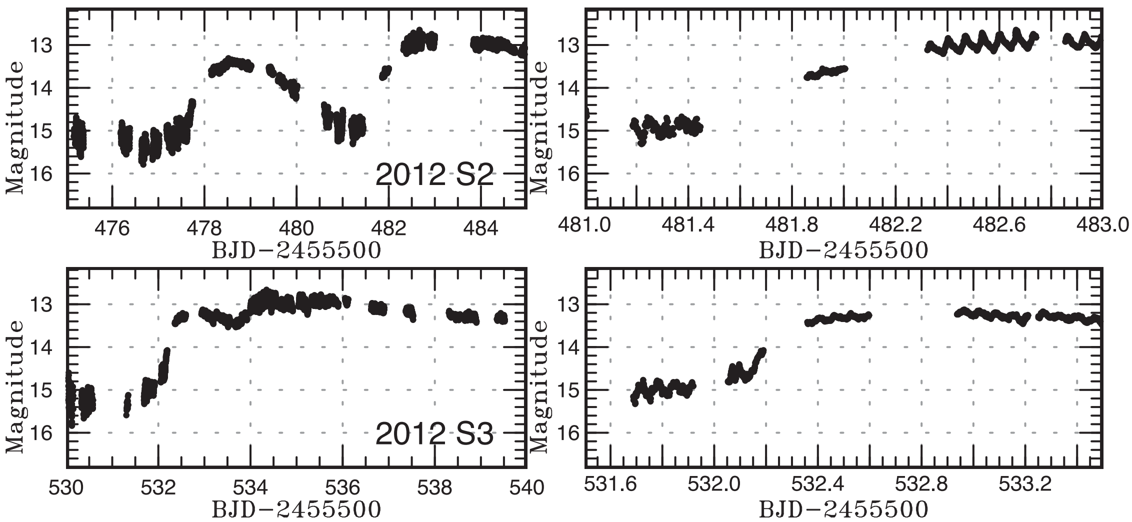

Fig. 4. Enlarged light curves of the rising stage of 2012 S2 (upper diagrams) and 2012 S3 (lower). The observation point is binned by 0.001 d. The left-hand diagrams show the precursors and the starts of superoutbursts. The right-hand diagrams show further enlarged light curves in order to show the superhump variations. Positive superhumps became dimmer and negative superhumps evolved.

outburst was JD (Julian day number) 2455622 and it persisted for 16 d. On JD 2455639, 14 d after the supermaximum, the decrease in brightness temporarily ceased and this object brightened by 0.5 mag. The superoutburst 2011 S3 is similar to 2011 S2.

Supercycle 2012 S0: Three normal outbursts (JD 2455900, 2455909, and 2455919) were caught before the first superoutburst where the time-resolved observations were performed in the 2012 season. According to monitoring observations reported to VSNET, the previous superoutburst (2012 S0) occurred around JD 2455869.

Supercycle 2012 S1: Because of lack of observations, it is unclear when the superoutburst 2012 S1 decayed, although the decline occurred between JD 2455941 and 2455943. Considering that the maximum of the superoutburst was around JD 2455929, the duration of the superoutburst was approximately 15 d.

Supercycle 2012 S2: The superoutburst 2012 S2 is an interesting case since the superoutburst was triggered during the decay of a normal outburst (the upper diagrams of figure 4). The duration of the superoutburst 2012 S2 was 14 d. After the superoutburst ended, this object had four normal outbursts (JD 2455998, 2456004, 2456012, and 2456022).

Supercycle 2012 S3: The superoutburst 2012 S3 is a typical superoutburst, which has a "shoulder" at its beginning (the lower diagrams of figure 4), as shown in Osaki and Kato (2013a). Despite lack of time-resolved observations in the late stage of the superoutburst 2012 S3, the VSNET data show that this object declined around JD 2456048–2456049. Thus the superoutburst 2012 S3 continued for 14–15 d. After the superoutburst decayed, four or five normal outbursts (maximum times: JD 2456051, 2456057, 2456063, 2456070, and 2456081) are detected. However, the fifth normal outburst (JD 2456081) may be a precursor outburst of the next superoutburst, 2012 S4. However, at any rate, the definite properties of these outbursts are not clear because of lack of observations. The properties of the next outburst (2012 S4) are also unclear for the same reason.

3.2 Frequency of normal outbursts

The number of normal outbursts in a supercycle in 2011 and 2012 was found to be mostly four and sometimes five (table 3). The case of five outbursts is exceptional and is discussed below. We reported in Paper I that the frequency of normal outbursts in the first supercycle of 2011 (i.e., 2011 S1) was lower than that found in previous observations of ER UMa, and we suggested that the existence of negative superhumps (and so the existence of a tilted disk) might suppress a frequent occurrence of normal outbursts. Zemko, Kato, and Shugarov (2013) pointed out that the number of normal outbursts in a supercycle of ER UMa varied between four and six over a long time scale, and also suggested that these differences are related to the appearance of negative superhumps. As discussed in the next subsection, it has turned out that all supercycles of ER UMa observed in 2011 and 2012 were accompanied by the negative superhump and thus they were Type L supercycles—for the definition of Type L and Type S supercycles, see Osaki and Kato (2013a).

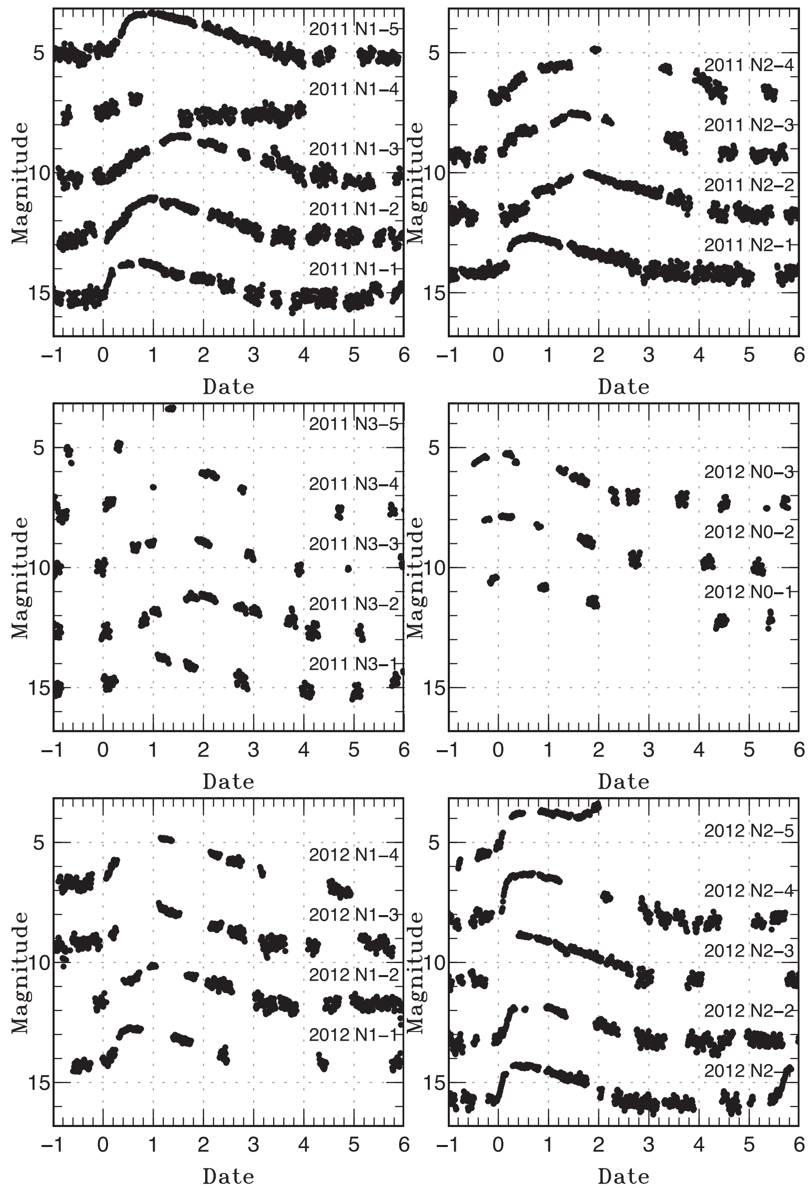

Fig. 5. Rising stage of normal outbursts. In the cycle of 2012 N0 (right-hand middle panel) the maximum of normal outbursts is set at zero, and in other cycles the start of normal outbursts is set at zero.

This trend continued almost unchangeably through the two seasons. Although five normal outbursts were observed between 2012 S1 and S2, the superoutburst 2012 S2 occurred at the declining stage of the fifth normal outburst. Thus this normal outburst was a precursor of the next superoutburst. Another exception is 2011 N1-4, which is discussed in a later subsection. Except for these cases, four normal outbursts were observed during one supercycle. The similar correlation between the appearance of negative superhumps and the frequency of normal outbursts in a supercycle was known in other SU UMa stars, V503 Cyg (Kato et al. 2002; Pavlenko et al. 2012) and V1504 Cyg (Osaki & Kato 2013a). In this respect, two exceptional cases of five normal outbursts in a supercycle are discussed here. As already mentioned for the individual supercycles, five normal outbursts occurred in supercycle 2012 S1 but the fifth has turned out to be a precursor normal outburst of superoutburst 2012 S2, and it may be regarded as a part of the next superoutburst. Another exception 2011 N1-4, which was found to be a minioutburst, is discussed in a later subsection.

3.2.1 Light-curve profile and rising rate of normal outbursts in a supercycle

Figure 5 illustrates variations in the light-curve profile of normal outbursts within each supercycle. Figure 6 exhibits the rising rate of normal outbursts within each supercycle. In the case of supercycle 2011 S1 (left-hand top panel of

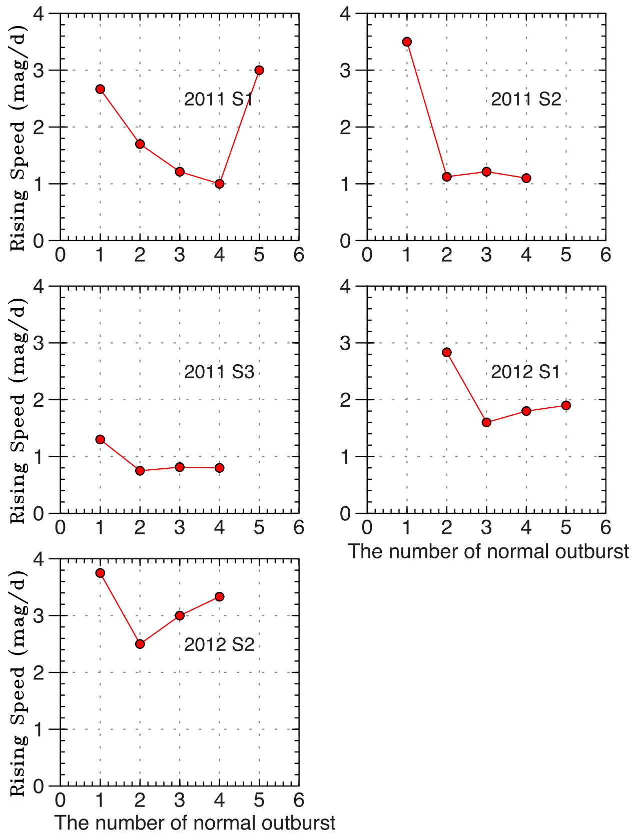

Fig. 6. Rising speed variation of each supercycle. Since the rising speed cannot be estimated because of the unclear timing of the start of outburst in some normal outbursts, such a rate is omitted. (Color online)

figure 5), we see that the rising rate to the maximum was getting slower with the development of the supercycle phase, except for the fifth normal outburst. We find in figure 5 that, generally speaking, the rising rate of the first normal outburst within each supercycle was faster than those of later normal ones. Two types of profile in outburst light curves are known to exist. One is that its rising rate is faster than its declining rate (i.e., rapid rise and slow decline), and the other is that the rising rate to the maximum is not so fast but more or less similar to the declining rate (i.e., the light-curve profile is more or less symmetric with respect to the maximum). In the disk-instability model for outbursts of dwarf novae, the former type of light curve is produced by the "outside-in" type outburst (or the type A outburst in Smak 1984) in which the transition to the hot state starts from the outer part of the accretion disk and the heating front propagates inward, while the latter type is produced by the "inside-out" outburst (type B in Smak 1984) in which the transition to the hot state starts from the inner part of the accretion disk. We find in these two figures that the first normal outburst in a supercycle looks like the "outside-in" type, while most of the other outbursts look like the "inside-out" type.

3.3 Negative superhumps

As shown in Paper I, negative superhumps are detected in ER UMa during superoutbursts as well as during normal outbursts and quiescence. The negative superhumps were clearly detected except for the early stage of the superoutburst. Their amplitude is 0.5–1.0 mag in quiescence. We also show the amplitude variation in flux units in figures 7 and 8. In these diagrams, 1 mag variation in 16 mag is normalized as 1. No dramatic change was associated with the change between quiescence and outburst seen in flux units (figures 7 and 8), as already pointed out in Osaki and Kato (2013a).

The valid interpretation of negative superhumps is the tilted accretion disk. The tilted disk shows retrograde precession, and Larwood (1998) presented an equation for q and ϵ_- for a retrograde precession of the tilted disk. Larwood (1998) indicates that the negative-superhump frequency is given by

$$\epsilon_-^* = \frac{\nu_{\rm orb} - \nu_{\rm nSH}}{\nu_{\rm orb}} = -\frac{3}{7}\frac{q}{\sqrt{1+q}}\left(\frac{R_{\rm d}}{A}\right)^{3/2}\cos\theta, \qquad (1)$$

where $\nu_{\rm nSH}$ and $\nu_{\rm orb}$ are the frequency for negative superhumps and the orbital frequency of the binary, respectively, and θ is the tilt angle of the disk to the binary's orbital plane. If θ is small, we can assume $\cos\theta \sim 1$, and that $\nu_{\rm nSH}$ can be determined by the disk radius, $R_{\rm d}$, for a specific system because q and A do not change in the observational time scale. In a real disk, $|\epsilon_-|$ represents the precession of the disk as a whole, to which precession rates from different radii contribute. Since the precession rates for smaller radii are smaller, the actual $|\epsilon_-|$ is smaller than what is expected for a ring in the outer radius of the disk. For more details, see the Appendix in Osaki and Kato (2013b).

Indeed, Osaki and Kato (2013b) indicated that the frequency of negative superhumps is a useful probe for studying the change of the radius of accretion disks in SU UMa-type dwarf novae through the analysis of V1504 Cyg. In this case, the frequency of negative superhumps varies systematically during a supercycle and the variation of the frequency is a good probe for the variation of the disk. Now we can observe the persistent negative superhump of ER UMa. Thus we have a good opportunity to investigate the variation of the disk radius through the negative-superhump period.

We analyzed the period of negative superhumps by two methods. In sub-subsection 3.3.1, we undertake the periodic analysis according to a traditional research method of dwarf novae; that is, drawing $O-C$ diagrams. And in sub-subsection 3.3.2, we adopt a new method called the least absolute shrinkage and selection operator

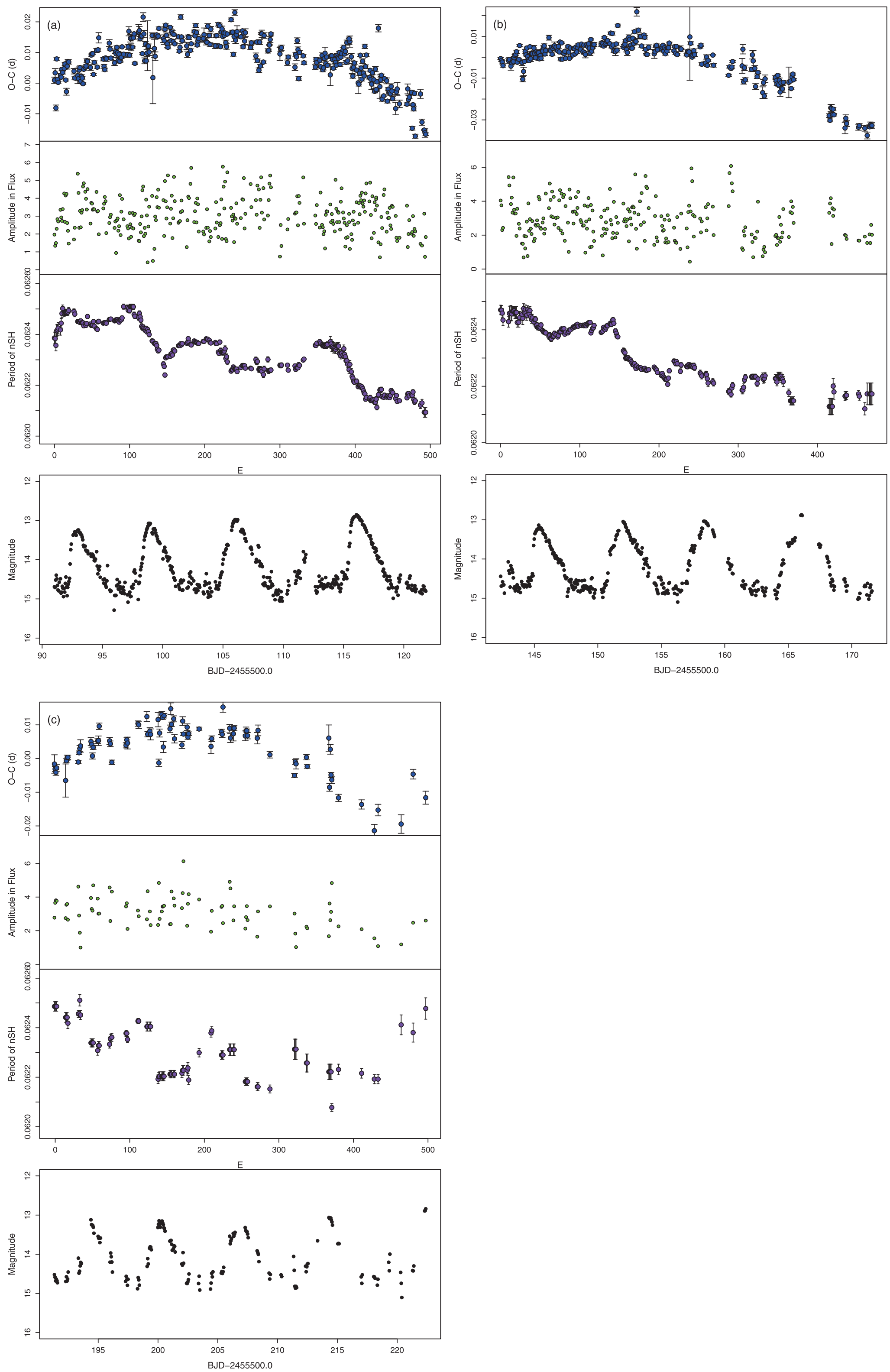

Fig. 7. $O-C$ diagram of negative superhumps, and related diagrams during each supercycle of 2011. Three panels (left-hand upper, right-hand upper, and left-hand lower) correspond to supercycles 2011 S1, 2011 S2, and 2011 S3. For each panel, top to bottom: (1) $O-C$ diagram of negative superhumps; (2) the amplitude of negative superhumps in flux; (3) the period of negative superhumps estimated by PDM analysis; (4) the light curve. The left-hand upper panel shows diagrams during 2011 S1–S2. The $O-C$ value is against the equation $2455591.020 + 0.062340\,E$. The right-hand upper panel shows diagrams during 2011 S2–S3. The $O-C$ value is against the equation $2455642.346 + 0.062339\,E$. The left-hand lower panel shows diagrams during 2011 S3–S4. The $O-C$ value is against the equation $2455691.405 + 0.062305\,E$. (Color online)

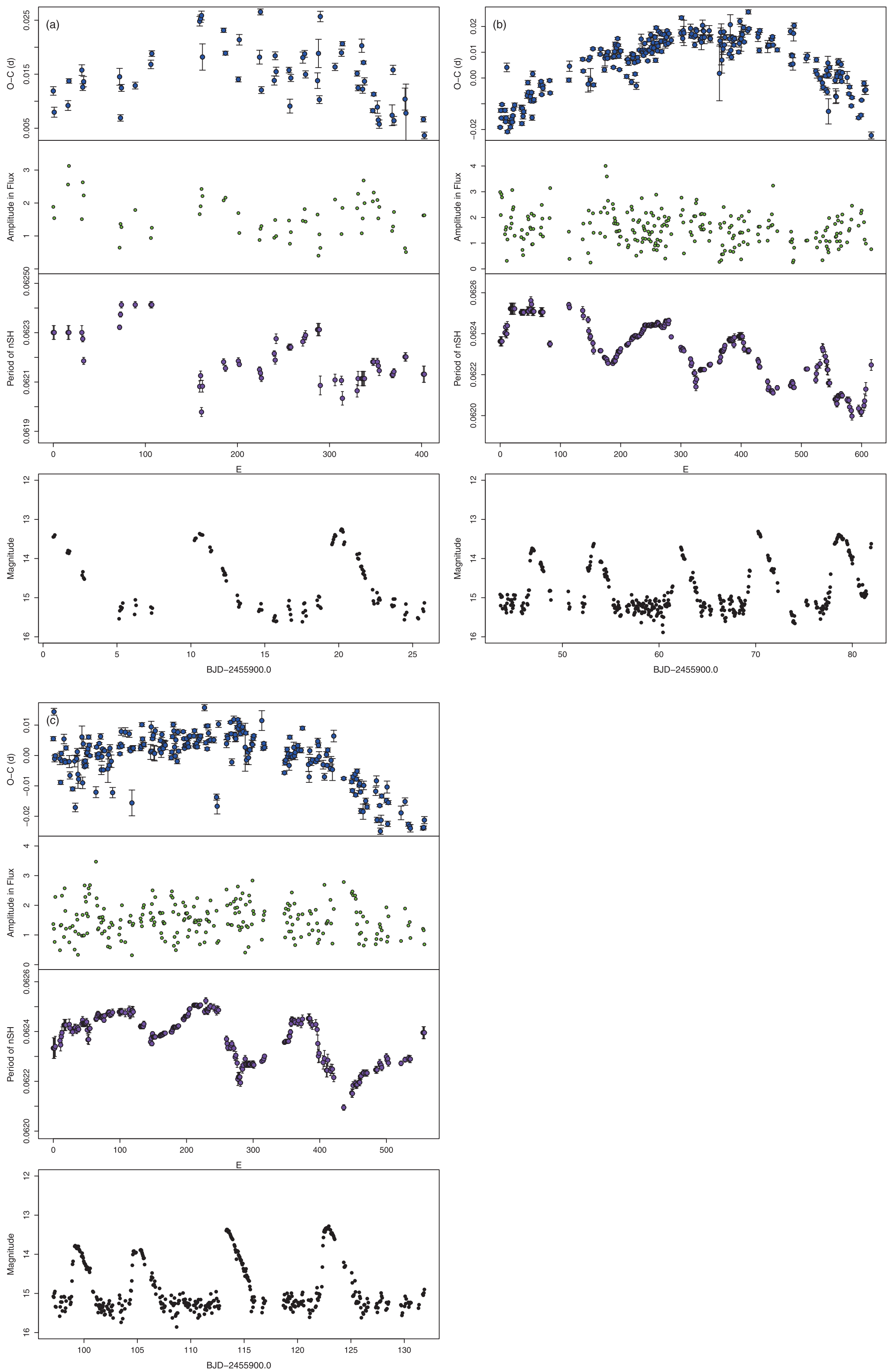

Fig. 8. $O-C$ diagram of negative superhumps, and related diagrams during each supercycle of 2012. Three panels (left-hand upper, right-hand upper, and left-hand lower) correspond to supercycles 2012 S0, 2012 S1, and 2012 S2. For each panel, top to bottom: (1) $O-C$ diagram of negative superhumps; (2) the amplitude of negative superhumps in flux; (3) the period of negative superhumps estimated by PDM analysis; (4) the light curve. The left-hand upper panel shows diagrams during 2012 S0. The $O-C$ value is against the equation $2455900.680 + 0.06223E$. The right-hand upper panel shows diagrams between 2012 S1 and 2012 S2. The $O-C$ value is against the equation $2455943.576 + 0.0623E$. The left-hand lower panel shows diagrams between 2012 S2 and 2012 S3. The $O-C$ value is against the equation $2455997.123 + 0.0624E$. (Color online)

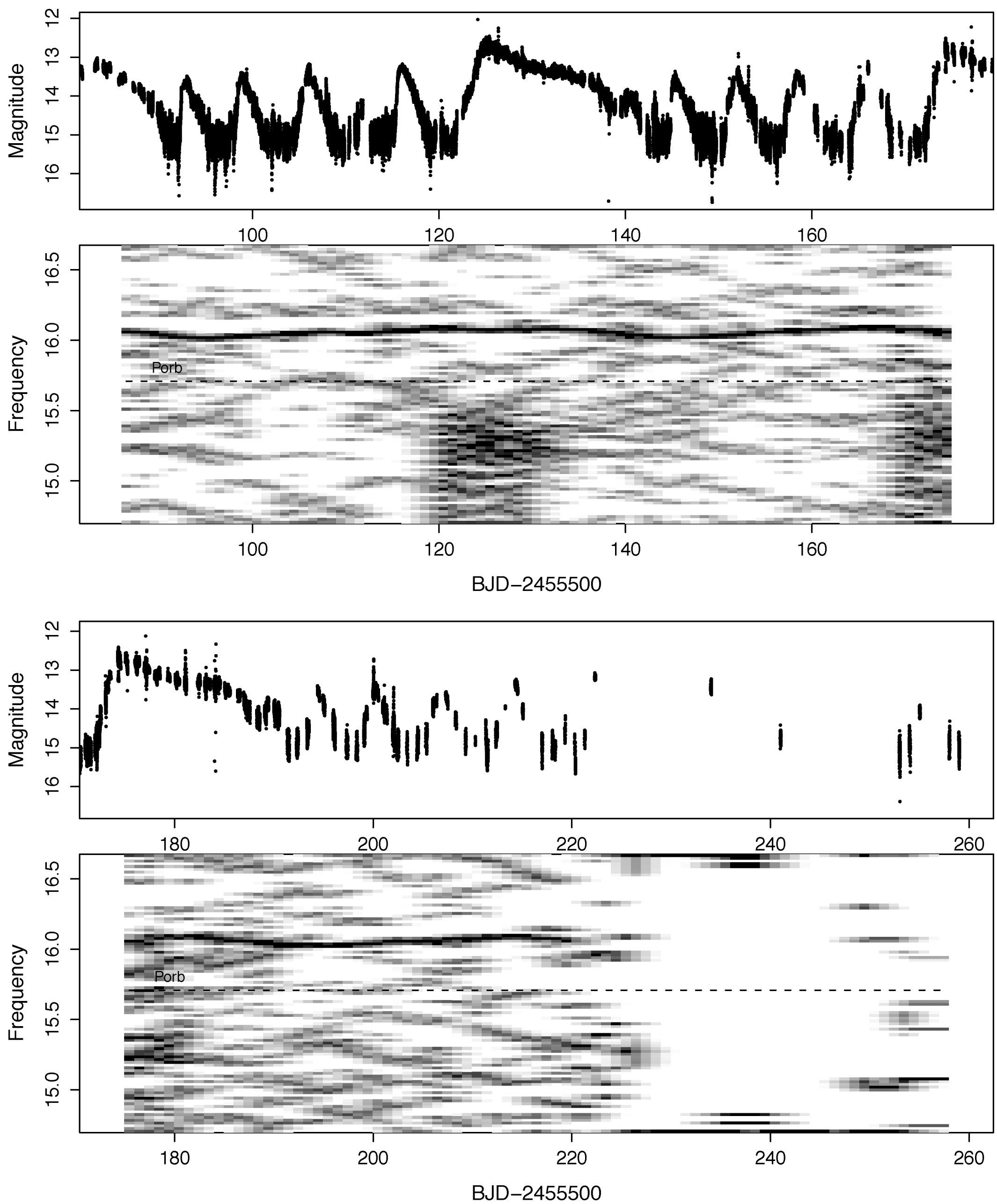

Fig. 9. Two-dimensional period analysis of ER UMa using Lasso in the 2011 season. In each panel, the top diagram is the light curve and the bottom diagram is the power spectrum. The width of the window is 10 d, and the time step is 1 d.

(Lasso and Tibshirani 1996) and perform the two-dimensional spectral analysis.

3.3.1 $O-C$ analysis

We estimated the maximum timing of negative superhumps the same as given in Kato et al. (2009) for data other than those in the superoutburst stage. The template for fitting the maximum time was an average of profiles of negative superhumps from data in quiescence between 2011 S1 and S2. (The periods of data used for the template are BJD 2455595–2455597.9, BJD 2455602–2455604.5, BJD 2455608–2455611.1, and BJD 2455618–2455622.0, and these data are folded by their mean negative-superhump period, 0.0623106 d.) We also estimated the amplitude of the negative superhumps and show it in the same figures.

The resultant $O-C$ diagrams are shown in figures 7 and 8. The $O-C$ diagrams indicate that the negative-superhump period gradually shortens as the next superoutburst is approaching. Namely, the derivative of the negative-superhump period, $\dot{P}_{\rm nSH}$, is negative between

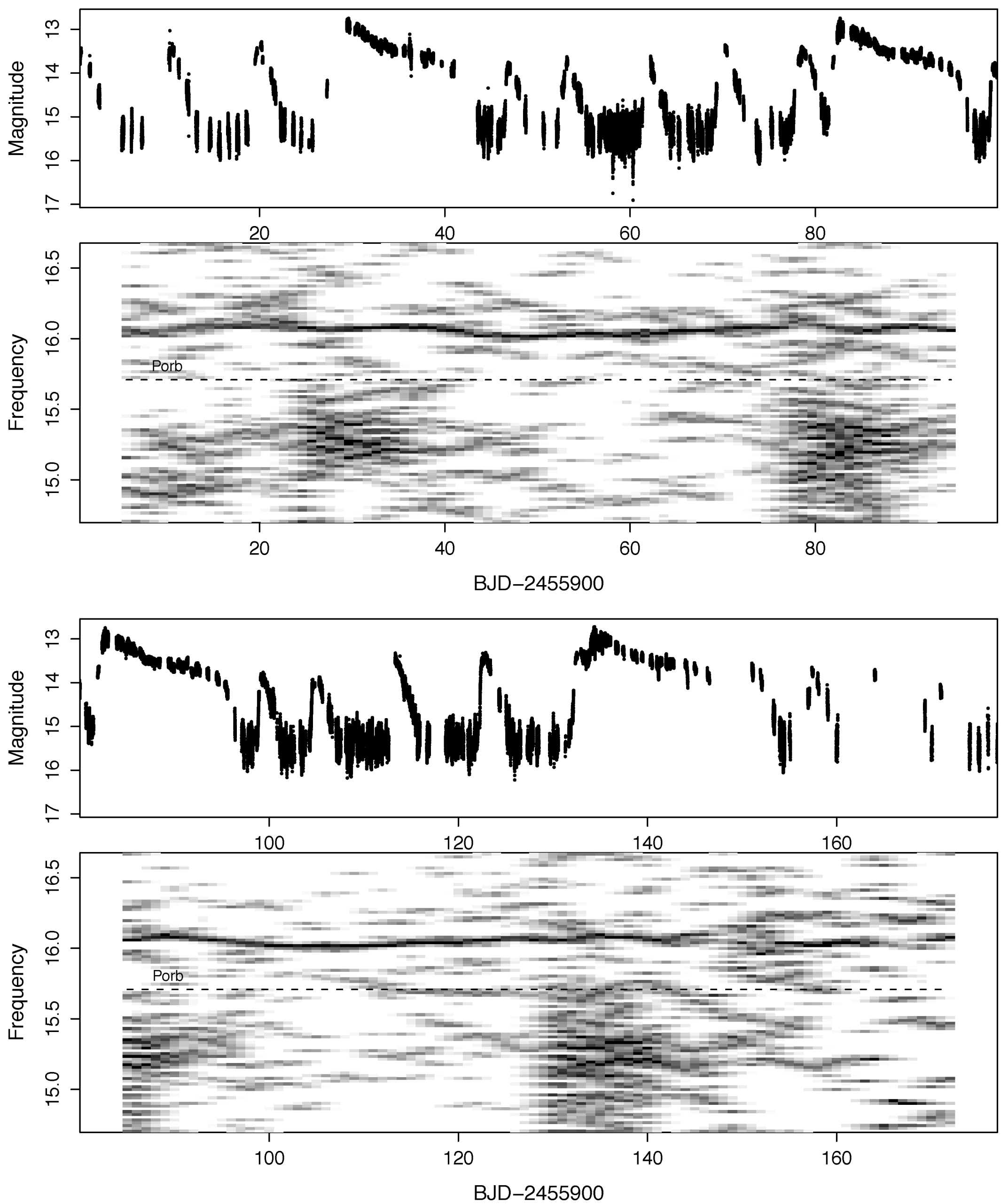

Fig. 10. Two-dimensional period analysis of ER UMa using Lasso in the 2012 season. In each panel, the top diagram is the light curve and the bottom diagram is the power spectrum. The width of the window is 10 d, and the time step is 1 d.

successive superoutbursts. The values of $\dot{P}_{\mathrm{nSH}}$ in 2011 are $-1.10(6) \times 10^{-5}$ (supercycle 2011 S1), $-1.32(4) \times 10^{-5}$ (supercycle 2011 S2) and $-1.04(11) \times 10^{-5}$ (supercycle 2011 S3). Meanwhile, the values of $\dot{P}_{\mathrm{nSH}}$ in 2012 are $-5(2) \times 10^{-6}$ (supercycle 2012 S0), $-9.7(4) \times 10^{-6}$ (supercycle 2012 S1), and $-7.7(6) \times 10^{-6}$ (supercycle 2012 S2). The absolute value of $\dot{P}_{\mathrm{nSH}}$ in 2011 is larger than that in 2012. However, the $O-C$ diagram shown in figure 8 has a more complicated structure on a shorter time scale, from the viewpoint of the normal outburst cycle. Namely, these $O-C$ curves are composed of multiple curves of convex shape, although the general appearance was concave on a long time scale, namely from the viewpoint of the supercycle. The third panel of each set in figures 7 and 8 shows the change of period during each supercycle. These values were calculated by the PDM analysis for a 5 d window width. Since the width is near the duration of normal outbursts, it is hard to detect observable changes of the period when an interval between two normal outbursts is short.

Since the period of the negative superhump is shorter than the orbital period, a small period of negative superhumps corresponds to a large negative fractional superhump deficit ϵ_-. Thus this result implies that the absolute value of ϵ_- gradually increases as the next superoutburst is approaching and, on a shorter time scale, the value of ϵ_- abruptly increases at the start of each normal outburst and gradually decreases until the next outburst starts. The increase of ϵ_- on a longer time scale is because the abrupt increase in the rising stage is larger than the gradual decrease in quiescence.

3.3.2 Lasso period analysis

Negative superhumps of ER UMa existed almost always during the observations of 2011 and 2012. We made a detailed analysis for the frequency variation of negative superhumps. We computed two-dimensional power spectra of the light curve of ER UMa. We used locally weighted polynomial regression (LOWESS: Cleveland 1979) on the observation data, in order to remove trends resulting from outbursts, with R software.[3] After that, we estimated the pulsed flux by multiplying the residual amplitude and LOWESS-smoothed light curve converted to the flux scale together. We used a 10 d width of the moving window, and 1 d as a time step because the data are not as contiguous as Kepler data. Since the window length is longer than the normal outburst cycle, periodic changes of shorter time scale are not well resolved. However, the periodic variation on a longer time scale is clearly seen.

We performed a period analysis called least absolute shrinkage and selection operator (Lasso: Tibshirani 1996), which was introduced into an analysis of astronomical time-series data (Kato & Uemura 2012; Kato & Osaki 2014). This method is very suitable for finding peaks in power spectra and highly effective in analyzing a rapid change of the period when dwarf novae are outbursting, because the Lasso analysis has the advantage that peaks in power spectra are very sharp, and is less affected by uneven sampling data than the Fourier analysis is.

The resultant two-dimensional power spectra are shown in figures 9 and 10. These figures show that clear negative-superhump signals were always detected during

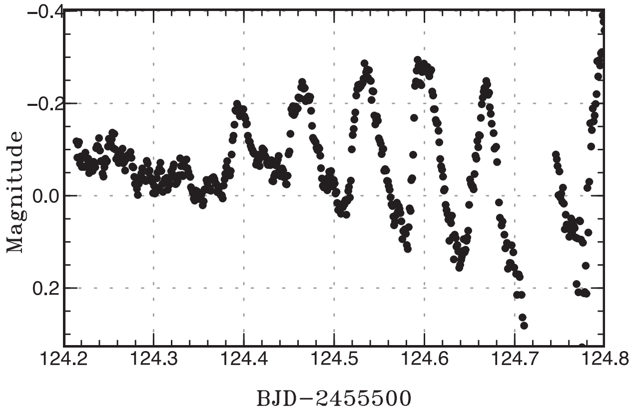

Fig. 11. Stage A superhump of 2011 S2, following LOWESS fitting and the subtraction of the negative-superhump signal. The observed data are binned to 0.001 d.

[3] ⟨http://www.r-project.org/index.html⟩.

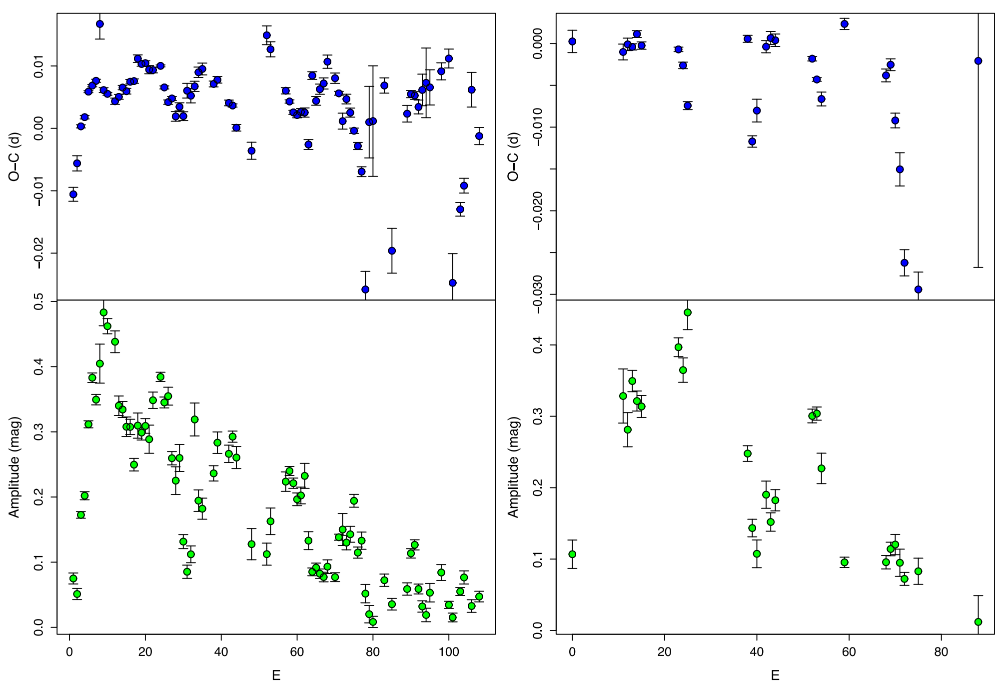

Fig. 12. $O-C$ diagrams of positive superhumps after subtracting negative superhumps of superoutbursts 2011 S2 and S3. The $O-C$ values are against the equations 2455624.392 + 0.065619 E (for 2011 S2) and 2455674.280 + 0.065619 E (for 2011 S3). (Color online)

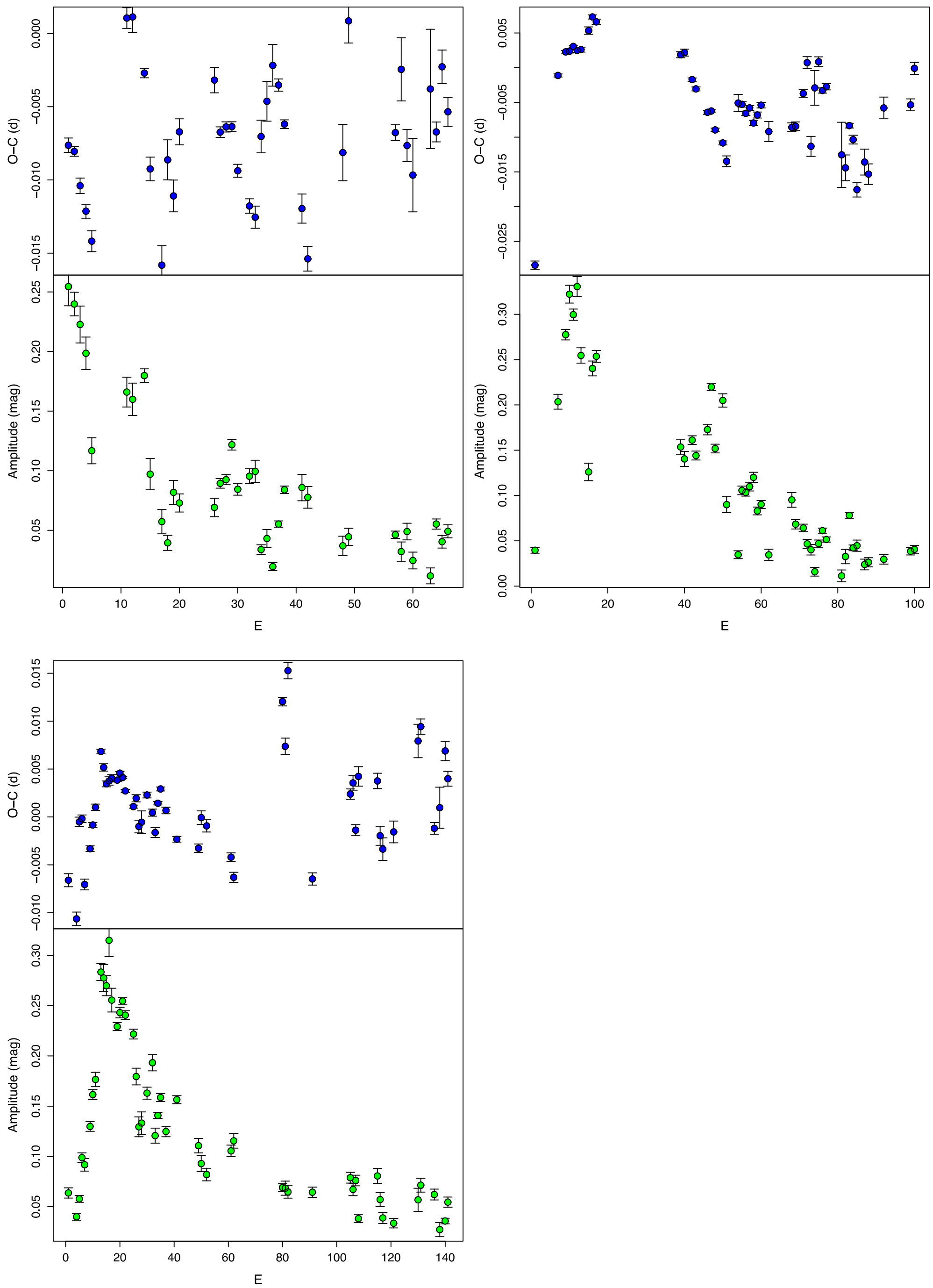

Fig. 13. $O-C$ diagrams of positive superhumps after subtracting negative superhumps of 2012 S1–S3. The values are against the equation of $2455924.094 + 0.065619E$ (for 2012 S1), $2455982.403 + 0.065619E$ (for 2012 S2), and $2456034.104 + 0.065710E$ (for 2012 S3). (Color online)

the two seasons, except for the early stage of superoutburst and the later phase of the 2011 season. The positive-superhump signal was detected only in the early stage of superoutburst. The frequency of negative superhumps was the smallest when the superoutburst ended, and increased toward the next superoutburst.

Interestingly, the Lasso diagram, especially in 2012, showed orbital modulation. Although we tried to determine a period of the orbital modulation, the signal was only partly seen, and so we could not find it.

Kato et al. (2014) and Osaki and Kato (2014) showed that the variation of negative-superhump periods in BK Lyn and ER UMa is not so large as that of ordinary SU UMa-type novae such as V344 Lyr and V1504 Cyg is, and suggested that this is because the outburst interval of these objects is extremely short.

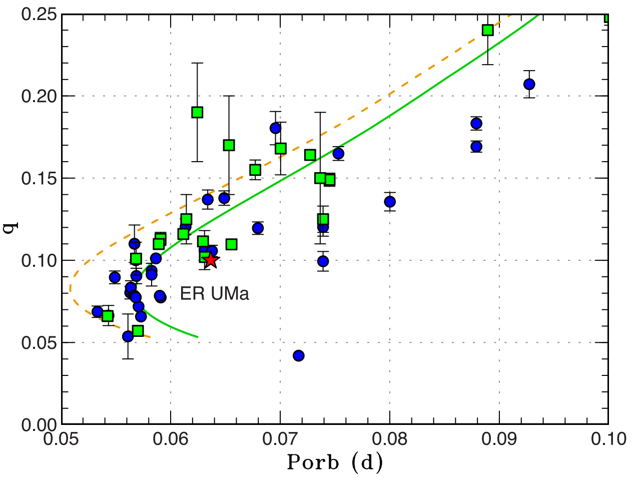

Fig. 14. Diagram of q versus P_{orb}. The data are derived from Kato and Osaki (2013). The filled circles represent q estimated from stage A superhumps. The filled squares represent q measured by eclipses. The filled star represents ER UMa. The dashed and solid curves represent the track of the standard evolutional theory and that of the modified evolutional theory (Knigge et al. 2011), respectively. (Color online)

3.3.3 Discussion concerning the periodic variation in negative superhumps

Both $O-C$ diagram and Lasso analysis show that the negative-superhump period shortens as the next superoutburst is approaching on a long time scale. However, on a short time scale, the period of negative superhumps tends to became longer in quiescence and abrupt shortening occurs at the start of normal outbursts. Due to a combination of these two effects, the negative-superhump period becomes shorter, accompanied as a whole by the smaller variations that are in accordance with normal outbursts outside the superoutburst stage. This corresponds to the global change of the $O-C$ diagram. The period change estimated by the PDM analysis is also in agreement with this result.

The theoretical relation implies that the increase of ν_{nSH} can be interpreted as an increase of R_{d}/A. Thus the change of negative-superhump period can be interpreted to mean that the radius of the disk increases when the normal outburst is triggered and that the accretion disk shrinks until the next normal outburst starts, although the increase is larger than the decrease. This change of disk radius is similar to that of V1504 Cyg shown in Osaki and Kato (2013b).

The TTI model suggests that the increase of disk radius at the start of an outburst is because of the conservation of angular momentum and the increased viscosity

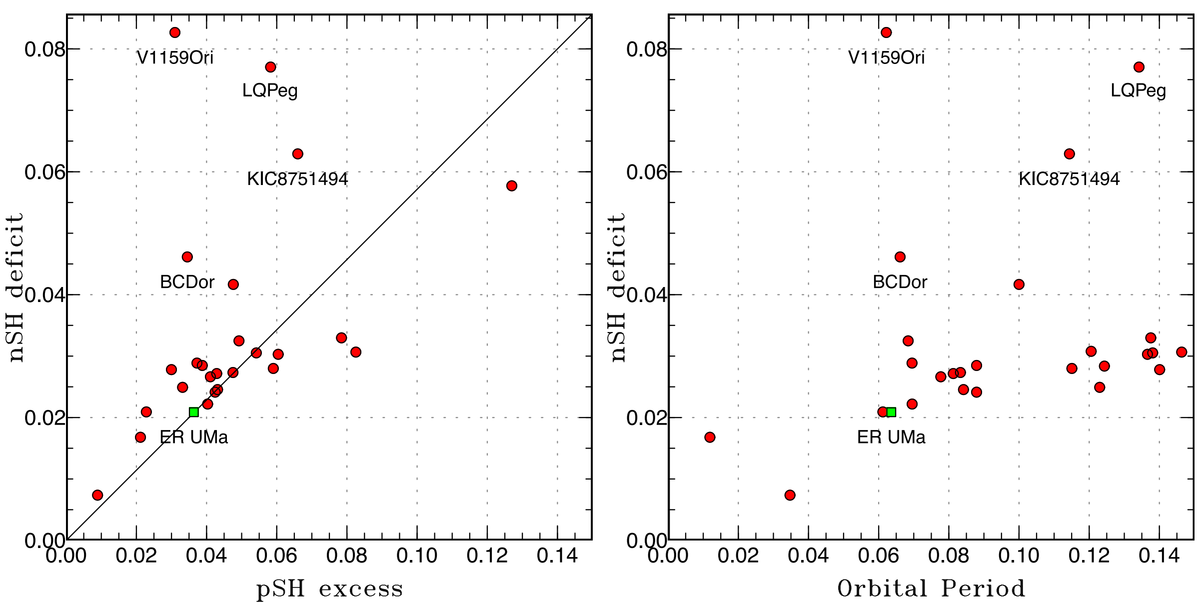

Fig. 15. Diagram of ϵ_+ versus ϵ_-. The solid line implies the theoretically predicted relation in the absence of the pressure effect. References: V1159 Ori (Patterson et al. 1995), AM CVn (Skillman et al. 1999; Patterson 1998, 1999), PX And (Stanishev et al. 2002), TV Col (Retter et al. 2003), BF Ara (Kato et al. 2003; Olech et al. 2007), V1405 Aql (Chou et al. 2001; Retter et al. 2002), AH Men (Patterson 1995), IR Gem (Fu et al. 2004), V503 Cyg (Harvey et al. 1995), TT Ari (Skillman et al. 1998; Andronov et al. 1999; Wu et al. 2002), V603 Aql (Patterson et al. 1997), RR Cha (Woudt & Warner 2002), V344 Lyr (Still et al. 2010; Osaki & Kato 2013b), V1504 Cyg (Osaki & Kato 2013a, 2013b), QU Aqr (Olech et al. 2009; Tramposch et al. 2005), BC Dor (Woudt et al. 2005), DW UMa (Stanishev et al. 2004; Patterson et al. 2005), V1974 Cyg (Olech 2002), KIC 8751494 (Kato & Maehara 2013), CSS 091121:033232+020439 (Woudt et al. 2012), and KIC 7524178 (Kato & Osaki 2014). (Color online)

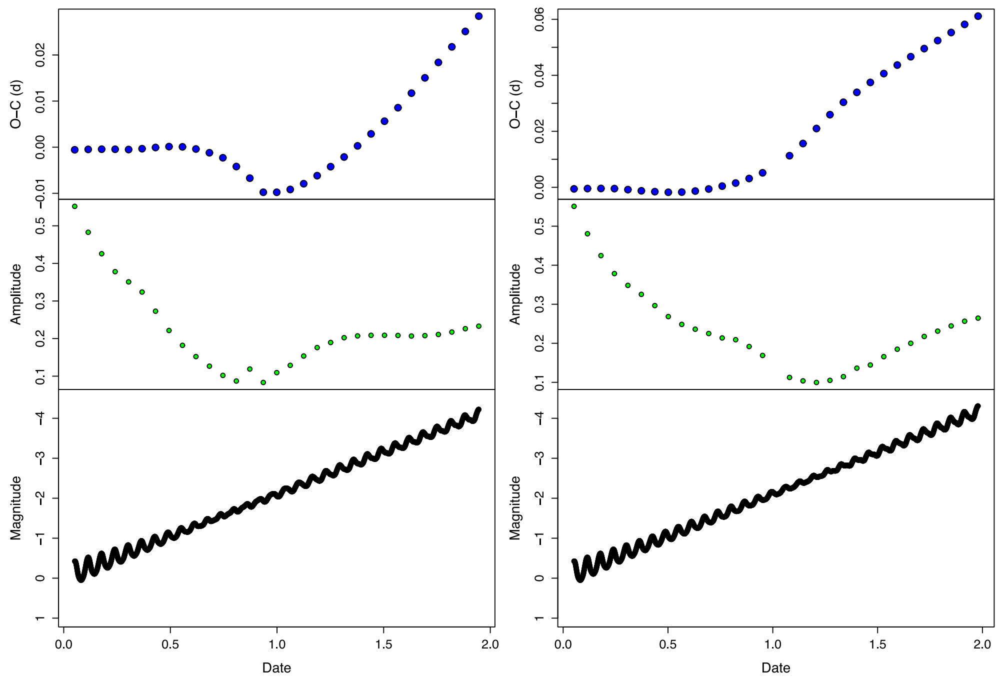

Fig. 16. Model calculation of the superimposition of negative and positive superhumps. In the left-hand panel, the positive superhump starts at phase 0 when the phase of the negative superhump is also 0. In the right-hand panel, the positive superhump starts at phase 0 when the phase of the negative superhump is 0.5. For each panel, the $O - C$ diagram and the amplitude variation of hump at the transition stage from positive to negative superhump are shown.

(Osaki 1989). After the outburst has finished, the disk radius shrinks until the next outburst starts. The negative-superhump period becomes shorter as the next superoutburst is approaching. Our result obeys this trend.

3.4 Positive superhumps

3.4.1 Stage A superhumps

ER UMa also shows positive superhumps. Through recent research (e.g., Kato et al. 2009), a superoutburst can be divided into three stages named "stage A, B, and C" after the change of the superhump period. Stage A corresponds to the evolving phase of the superhump, when the tidal instability is limited to the 3:1 resonance radius. After superhumps after stage B, the eccentric wave spreads to the inner region of the disk and the pressure effect appears (Osaki & Kato 2013b). Thus, the stage A superhump period gives us the mass ratio q of the system (Kato & Osaki 2013). It is very useful for detecting stage A superhumps and estimating the period.

Kato and Osaki (2013) suggested an explanation of why stage A superhumps are difficult of detection in ER UMa-type dwarf novae. In ER UMa-type dwarf novae, the superoutburst is not necessarily triggered by a normal outburst but by the eccentric instability—called Case C outburst in Osaki and Meyer (2003). In such a case, the pressure effect has already been strong at the start of a superoutburst and the method of estimating q by the stage A superhump period may not be applicable. However, in superoutbursts during our observations, positive superhumps were triggered by normal outbursts the same as in usual SU UMa-type objects. Therefore the existence of stage A superhumps is expected.

As seen in figures 9 and 10, negative and positive superhumps coexist during the superoutburst. It is supposed that positive superhumps are caused by prograde precession of the elliptical disk and negative superhumps are caused by retrograde precession of the tilted disk. The coexistence of positive and negative superhumps suggests that the disk is eccentric and tilts at the same time.

This coexistence of negative and positive superhumps constitutes an obstacle to an estimation of maximum timings of positive superhumps. We have to subtract the variation of negative superhumps.

We adopted an averaged light curve of negative superhumps for the subtraction. First we subtracted it from the original light curve translated into the flux scale. After that, the averaged light curve formed a subset of data during one beat cycle. This averaged light curve on the flux scale was translated into the magnitude scale again. The subtracted light curve is shown in figure 11.

The O − C diagrams of five superoutbursts after subtraction of negative superhumps are shown in figures 12 and 13. In 2011 S1, negative superhumps were dominant at the start of the time-resolved observation, and thus the $O - C$ curve of positive superhumps could not be drawn.

Among five superoutbursts, stage A superhumps were detected in three superoutbursts (2011 S2, 2012 S2, and 2012 S3). These detections were based on the longer

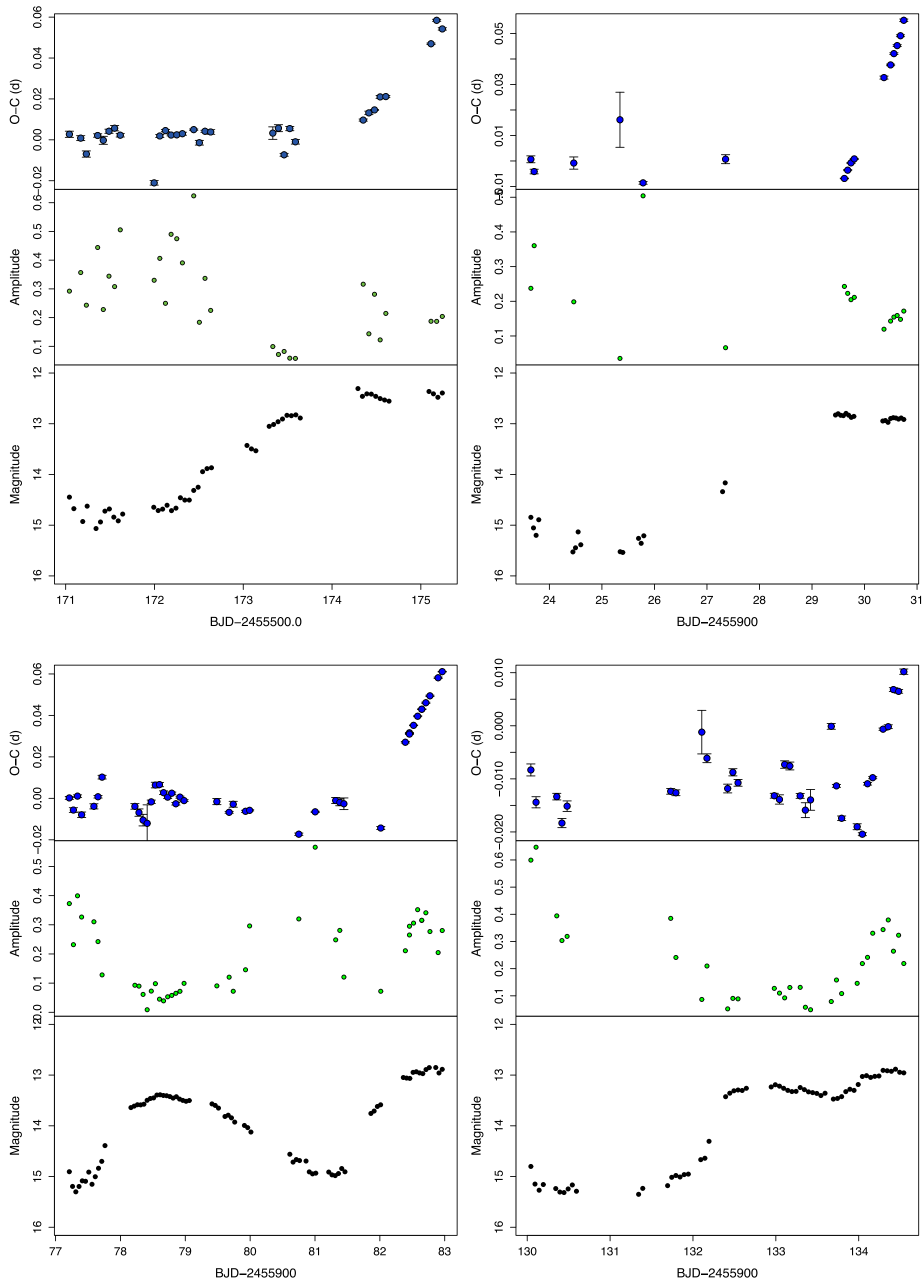

Fig. 17. $O-C$ diagram, amplitude variation, and light curve (0.01 d binned) during the rising stage of superoutbursts. The left-hand upper panel is the diagram of superoutburst 2011S3. The value of $O-C$ diagram is against the equation 2455671.039+0.0622 E. The right-hand upper panel is the diagram of superoutburst 2012S1. The value of $O-C$ diagram is against the equation 2455923.646+0.0622 E. The left-hand lower panel is the diagram of superoutburst 2012S2. The value of $O-C$ diagram is against the equation 2455977.211+0.0622 E. The right-hand lower panel is the diagram of superoutburst 2012S3. The value of $O-C$ diagram is against the equation 2456030.063+0.0622 E.

superhump period and the increase of the amplitude of superhumps in the earliest stage of the superoutburst. For instance, the amplitude of positive superhumps in 2011 S2 increased to 0.50 mag at $E = 10$ (figure 12). In 2011 S3 and 2012 S1, it was difficult to estimate the stage A superhump period because of lack of observations. After the amplitude of positive superhumps reached a maximum, this amplitude became gradually smaller. These superhumps can be regarded as stage B superhumps. However the perfect subtraction of negative superhumps, especially in the later stage, is difficult. The profile of superhumps of ER UMa during its superoutburst does not seem to be a simple superposition of positive and negative superhumps.

Then we obtained the periods of stage A superhumps. For the data of 2011 S2, a PDM analysis yielded a stage A superhump period of 0.06604(9) d. Similarly the stage A superhump period is estimated to be 0.06570(2) d in 2012 S2 and 0.06624(4) d in 2012 S3. With those data, an estimated q is 0.100(6) by the method of Kato and Osaki (2013). Data of the other superoutbursts indicate somewhat different values of 0.088 (2012 S2) and 0.114 (2012 S3). Using an average of these values, we found q of ER UMa to be 0.100(15).

3.4.2 System property and evolutionary state

The estimated value of q, 0.100(15), suggests that ER UMa is on the standard evolutionary track in Knigge, Baraffe, and Patterson (2011) since the orbital period is 0.06366 d (figure 14). Our results indicate there is no evidence that ER UMa is in an evolutional stage different from ordinary CVs, although $\dot{M}$ of ER UMa is much higher than those of other SU UMa-type dwarf novae with a similar orbital period.

Hellier (2001b) suggested that the unusual behavior of ER UMa-type novae (rapid recurrence of normal outbursts) or WZ Sge-type objects (rebrightenings) may be explained if these objects have an extremely low q (i.e., near the period minimum or period bouncers) and the thermal and tidal instabilities are decoupled due to weak tidal force. Our present result indicates that, at least for ER UMa itself, this is not the case. We consider that there is no necessity to consider decoupling of the thermal and tidal instabilities for ER UMa as shown by Osaki (1995a), in which the behavior of ER UMa can be reproduced by increasing $\dot{M}$, while there remains a possibility of decoupling for RZ LMi (Osaki 1995b). Determination of the orbital period and detection of stage A superhumps for RZ LMi and DI UMa are desired to solve this problem.

3.4.3 Relation between positive and negative superhumps

The left-hand panel of figure 15 shows the relation between the negative-superhump period and the positive-superhump period for the systems which show both superhumps. Theoretically, the ratio of the negative-superhump period to the positive-superhump period is 4/7 without the pressure effect. Most of the systems obey this relation. Among the systems deviating from the theoretical relation, KIC 8751494 can be explained by the pressure effect (Kato & Maehara 2013). The negative superhump of V1159 Ori may not be a true negative superhump, but an "impulsive negative superhump" (Osaki & Kato 2013b).[4]

Our value for ER UMa is especially consistent with this relation. Although Gao et al. (1999)'s value is far shorter than ours and the theoretical prediction, this may be also an "impulsive negative superhump." The right-hand panel of figure 15 shows the relation between the orbital period and the negative-superhump deficit.

[4] This phenomenon was also described in Wood et al. (2011).

3.5 Transition from negative superhump to positive superhump

In Paper I, we reported that the maximum timings of negative and positive superhumps developed continuously and that there was no phase shift between them. This implies that the source of negative and positive superhumps is the same. A similar trend was also seen in other rising stages. However, this is unclear because the amplitude of superhumps in the transition stage was small. We tested this trend in model calculations.

We assumed: the positive superhump develops in the rising stage of the superoutburst; the constant amplitude in flux of the negative superhump is 0.7 mag in quiescence; the rising rate of mean magnitude is 2.1 mag d^{-1}; positive superhumps start their development four cycles after their rising starts; after positive superhumps appear, the amplitude of positive superhumps develops at a speed of 0.15 mag d^{-1}. For the profile of negative and positive superhumps, the template profiles used for nonlinear fitting were adopted.

The resultant diagrams are shown in figure 16. In the left-hand panel, the phases of negative and positive superhumps are continuous when the positive superhumps start to develop. In the right-hand panel, the phases of negative and positive superhumps differ by 0.5. Both diagrams show the decrease of amplitude variation when the positive superhumps begin to develop. Furthermore, the negative-superhump phase evolves into the positive superhump smoothly in both $O-C$ diagrams. In the left-hand panel of figure 16, $O-C$ variation does not show a small, smooth transition from negative superhump to positive superhump, but shows a more complex structure. This is caused by the superimposition of the maxima of negative and positive superhumps. However, since the amplitude of positive superhumps is small, the shift of the $O-C$ value is small.

The $O-C$ diagram of the rising stage of each superoutburst is shown in figure 17. These $O-C$ diagrams imply that the negative and positive superhumps are continuous without phase shift the same as in the right-hand panel of figure 16. This result suggests the position where the positive superhump is not randomly excited in relation to negative superhumps.

This result would not be expected if negative superhumps arise from the varying release of the potential energy on a tilted disk and if the phase of the tilt is random to the observer when positive superhumps start to grow. Neither our understanding of the origin of negative superhumps nor the statistics may be sufficient to prove whether or not the positive superhump is randomly excited in relation to negative superhumps. Further systematic observations of the rising stage of superoutbursts are required.

4 Conclusion

We observed the SU UMa-type dwarf nova ER UMa in 2011 and 2012 by VSNET worldwide campaign, and we obtained data for 307 nights in a span of two years. We detected persistent negative superhumps during the superoutbursts as well as during normal outbursts and quiescence in both seasons. We analyzed these data and obtained the following major findings:

(1) We succeeded in making observations over three supercycles of this star in 2011 and also over three supercycles in 2012. The star showed persistent superhumps in both seasons.

(2) We analyzed periodic variations of negative superhumps in a supercycle of this star by the $O-C$ analysis, PDM analysis, and Lasso analysis. We found that the period of negative superhumps between two successive superoutbursts decreases secularly from the end of a superoutburst to the next superoutburst on a longer time scale of supercycle. Superimposed on this long time-scale trend, a shorter time-scale variation in the negative-superhump period occurred within a normal outburst cycle in the sense that the period was shortened when a normal outburst occurred and the period became longer during quiescence. When the next supercycle started, the period of negative superhumps returned to the value when the previous supercycle started. Thus it varied cyclically with the same supercycle period as that of the light curve. This variation was indicated as a result of the variation in the disk radius, and the disk radius was the smallest at the end of a superoutburst. The variation in the disk radius inferred from our analysis of ER UMa is in agreement with the predicted variation of the disk radius by the TTI theory.

(3) The rising rate to the maximum of normal outburst varied during one supercycle. The rising rate of the first normal outburst within a supercycle was found to be faster than the later ones. This suggests that the first normal outburst may be most likely of the "outside-in" type while the later ones may be of the "inside-out" type. The occurrence of the "inside-out" type outbursts in ER UMa may be understood as being due to the mass supply from the secondary to the inner part of the disk when the disk tilted.

(4) Negative superhumps and positive superhumps coexisted during the superoutburst although the signal of the negative superhump was marginal in the first few days of the superoutburst. By subtracting the signal of the negative superhumps, we obtained the $O-C$ diagram for the positive superhumps, and by doing so we were able to distinguish stage A from stage B. A simple combination of the positive and negative superhumps was not sufficient to reproduce the complex profile variation.

(5) The number of normal outbursts in a supercycle of ER UMa in 2011 and 2012 was found to be mostly four, which was smaller than that on other occasions when negative superhumps were not observed, and to be consistent with those reported for ER UMa by Zemko, Kato, and Shugarov (2013) and for V1504 Cyg by Osaki and Kato (2013a). This can be understood as a result of the tilted disk; when the disk is tilted, the gas stream coming from the secondary arrives at the inner region of the disk rather than at the disk edge and this reduces the frequent occurrence of the "outside-in" type normal outbursts.

(6) Some of the superoutbursts were triggered by the normal outbursts (i.e., precursor outbursts). Positive superhumps started to grow during the declining part of the precursor in such superoutbursts. The phases of maxima were found to be continuous when a transition from the negative superhump to the positive superhump occurred.

(7) We succeeded in detecting stage A superhumps for the first time in ER UMa-type dwarf novae during the precursor parts of three superoutbursts. Using the period of stage A superhumps, we estimated q of ER UMa to be 0.100(15). The estimated q and the known orbital period imply that ER UMa itself is in the standard evolutionary track of cataclysmic variable stars. However, the mass transfer rate, $\dot{M}$, of ER UMa, inferred from its short supercycle length and frequent occurrence of normal outbursts, is much higher than that of other SU UMa-type dwarf novae with a similar orbital period.

Acknowledgments

The authors are grateful to the observers of the VSNET Collaboration and VSOLJ observers, who contributed observations covering long-term variations of ER UMa as long as two years.

This work was partly supported by a Grant-in-Aid "Initiative for High-Dimensional Data-Driven Science through Deepening of Sparse Modeling" from the Ministry of Education, Culture, Sports, Science and Technology (MEXT) of Japan, and a Grant-in-Aid for the Global COE Program "The Next Generation of Physics, Spun from Universality and Emergence" from MEXT. We are very grateful to the referee, Y. Osaki.

Supporting information

Additional Supporting Information may be found in the online version of this article:

Tables 4–10

Please note: Oxford University Press are not responsible for the content or functionality of any supporting materials supplied by the authors. Any queries (other than missing material) should be directed to the corresponding author for the article.

References

Andronov, I. L., et al. 1999, AJ, 117, 574
Chou, Y., Grindlay, J. E., & Bloser, P. F. 2001, ApJ, 549, 1135
Cleveland, W. S. 1979, J. Amer. Statistical Assoc., 74, 829
Fu, H., Li, Z.-Y., Leung, K.-C., Zhang, Z.-S., Li, Z.-L., & Gaskell, C. M. 2004, Chin. J. Astron. Astrophys., 4, 88
Gao, W., Li, Z., Wu, X., Zhang, Z., & Li, Y. 1999, ApJ, 527, L55
Harvey, D., Skillman, D. R., Patterson, J., & Ringwald, F. A. 1995, PASP, 107, 551
Hellier, C. 2001a, Cataclysmic Variable Stars: How and Why they Vary (Berlin: Springer-Verlag)
Hellier, C. 2001b, PASP, 113, 469
Hirose, M., & Osaki, Y. 1990, PASJ, 42, 135
Kato, T., et al. 2009, PASJ, 61, S395
Kato, T., et al. 2014, PASJ, 66, 30
Kato, T., Bolt, G., Nelson, P., Monard, B., Stubbings, R., Pearce, A., Yamaoka, H., & Richards, T. 2003, MNRAS, 341, 901
Kato, T., Ishioka, R., & Uemura, M. 2002, PASJ, 54, 1029
Kato, T., & Kunjaya, C. 1995, PASJ, 47, 163
Kato, T., & Maehara, H. 2013, PASJ, 65, 76
Kato, T., Nogami, D., Baba, H., Masuda, S., Matsumoto, K., & Kunjaya, C. 1999, in Disk Instabilities in Close Binary Systems, ed. S. Mineshige & J. C. Wheeler (Tokyo: Universal Academy Press), 45
Kato, T., & Osaki, Y. 2013, PASJ, 65, 115
Kato, T., & Osaki, Y. 2014, PASJ, 66, L5
Kato, T., & Uemura, M. 2012, PASJ, 64, 122
Kato, T., Uemura, M., Ishioka, R., Nogami, D., Kunjaya, C., Baba, H., & Yamaoka, H. 2004, PASJ, 56, S1
Kjurkchieva, D., & Marchev, D. 2010, Publ. Astron. Obs. Belgrade, 90, 147
Knigge, C., Baraffe, I., & Patterson, J. 2011, ApJS, 194, 28
Larwood, J. 1998, MNRAS, 299, L32
Nogami, D., Kato, T., Masuda, S., & Hirata, R. 1995, IBVS, 4155
Ohshima, T., et al. 2012, PASJ, 64, L3 (Paper I)
Olech, A. 2002, Acta Astron., 52, 273
Olech, A., Rutkowski, A., & Schwarzenberg-Czerny, A. 2007, Acta Astron., 57, 331
Olech, A., Rutkowski, A., & Schwarzenberg-Czerny, A. 2009, MNRAS, 399, 465
Osaki, Y. 1989, PASJ, 41, 1005
Osaki, Y. 1995a, PASJ, 47, L11
Osaki, Y. 1995b, PASJ, 47, L25
Osaki, Y. 1996, PASP, 108, 39
Osaki, Y., & Kato, T. 2013a, PASJ, 65, 50
Osaki, Y., & Kato, T. 2013b, PASJ, 65, 95
Osaki, Y., & Kato, T. 2014, PASJ, 66, 15
Osaki, Y., & Meyer, F. 2003, A&A, 401, 325
Patterson, J. 1995, PASP, 107, 657
Patterson, J. 1998, PASP, 110, 1132
Patterson, J. 1999, in Disk Instabilities in Close Binary Systems, ed. S. Mineshige, & J. C. Wheeler (Tokyo: Universal Academy Press), 61
Patterson, J., et al. 2005, PASP, 117, 1204
Patterson, J., Jablonski, F., Koen, C., O'Donoghue, D., & Skillman, D. R. 1995, PASP, 107, 1183
Patterson, J., Kemp, J., Saad, J., Skillman, D. R., Harvey, D., Fried, R., Thorstensen, J. R., & Ashley, R. 1997, PASP, 109, 468
Pavlenko, E. P., Samsonov, D. A., Antonyuk, O. I., Andreev, M. V., Baklanov, A. V., & Sosnovskij, A. A. 2012, Astrophysics, 55, 494
Retter, A., Chou, Y., & Bedding, T. 2002, in ASP Conf. Ser., 261, The Physics of Cataclysmic Variables and Related Objects, ed. B. T. Gänsicke et al. (San Francisco: ASP), 527
Retter, A., Hellier, C., Augusteijn, T., Naylor, T., Bedding, T. R., Bembrick, C., McCormick, J., & Velthuis, F. 2003, MNRAS, 340, 679
Ringwald, F. A., Velasco, K., Roveto, J. J., & Meyers, M. E. 2012, New Astron., 17, 433
Robertson, J. W., Honeycutt, R. K., & Turner, G. W. 1995, PASP, 107, 443
Skillman, D. R., et al. 1998, ApJ, 503, L67
Skillman, D. R., Patterson, J., Kemp, J., Harvey, D. A., Fried, R. E., Retter, A., Lipkin, Y., & Vanmunster, T. 1999, PASP, 111, 1281
Smak, J. 1984, Acta Astron., 34, 161
Smak, J. 1985, Acta Astron., 35, 357
Stanishev, V., Kraicheva, Z., Boffin, H. M. J., & Genkov, V. 2002, A&A, 394, 625
Stanishev, V., Kraicheva, Z., Boffin, H. M. J., Genkov, V., Papadaki, C., & Carpano, S. 2004, A&A, 416, 1057
Still, M., Howell, S. B., Wood, M. A., Cannizzo, J. K., & Smale, A. P. 2010, ApJ, 717, L113
Tibshirani, R. 1996, J. R. Statistical Soc. B, 58, 267
Tramposch, J., Homer, L., Szkody, P., Henden, A., Silvestri, N. M., Yirak, K., Fraser, O. J., & Brinkmann, J. 2005, PASP, 117, 262
Udalski, A. 1988, Acta Astron., 38, 315
Warner, B. 1995, Cataclysmic Variable Stars (Cambridge: Cambridge University Press)
Whitehurst, R. 1988, MNRAS, 232, 35
Wood, M. A., & Burke, C. J. 2007, ApJ, 661, 1042
Wood, M. A., Still, M. D., Howell, S. B., Cannizzo, J. K., & Smale, A. P. 2011, ApJ, 741, 105
Woudt, P. A., & Warner, B. 2002, MNRAS, 335, 44
Woudt, P. A., Warner, B., de Budé, D., Macfarlane, S., Schurch, M. P. E., & Zietsman, E. 2012, MNRAS, 421, 2414
Woudt, P. A., Warner, B., & Spark, M. 2005, MNRAS, 364, 107
Wu, X., Li, Z., Ding, Y., Zhang, Z., & Li, Z. 2002, ApJ, 569, 418
Zemko, P., Kato, T., & Shugarov, Yu. S. 2013, PASJ, 65, 54